Copy 5
RM A52J06

NACA RM A52J06

NACA

RESEARCH MEMORANDUM

CORRELATION OF PREDICTED AND EXPERIMENTAL LATERAL OSCILLATION CHARACTERISTICS FOR SEVERAL AIRPLANES

By Donovan R. Heinle and Walter E. McNeill

Ames Aeronautical Laboratory
Moffett Field, Calif.

NATIONAL ADVISORY COMMITTEE
FOR AERONAUTICS

WASHINGTON

December 15, 1952

[redacted]

NATIONAL ADVISORY COMMITTEE FOR AERONAUTICS

RESEARCH MEMORANDUM

CORRELATION OF PREDICTED AND EXPERIMENTAL LATERAL OSCILLATION CHARACTERISTICS FOR SEVERAL AIRPLANES

By Donovan R. Heinle and Walter E. McNeill

SUMMARY

An investigation of the accuracy of a presently used method for predicting the dynamic lateral oscillatory characteristics of airplanes has been made. This study involved the comparison of controls-fixed flight-test data from several current fighter-type jet airplanes with the calculated values of period and damping for these airplanes. These calculations were made from geometric and mass characteristics and aerodynamic derivatives derived from geometric characteristics and wind-tunnel data.

For the airplanes included in this investigation, it was found that the dynamic lateral oscillatory characteristics could be predicted with reasonable accuracy by use of the geometric and mass characteristics and static wind-tunnel data. Where discrepancies did exist between experimental and calculated data, they were attributable to control motion or to parameter inaccuracies in the calculations. It was found that, for airplanes involving deviations from the conventional configurations, special techniques for obtaining the dynamic derivatives such as dynamic wind-tunnel tests are advisable.

INTRODUCTION

With the increasing complexity and cost of the modern airplane, it becomes desirable to predict as far as possible in advance of its completion approximately what the flight stability characteristics will be. Thus any expected deficiencies may be noted and their possible corrections may be applied early in the development and construction of the airplane to minimize time loss and expense. The extension of flight to the higher altitudes and speeds experienced in recent years has made it an increasingly greater problem to produce aircraft that perform within the limits

[redacted]

of desirable stability characteristics, so the prediction of these stability characteristics becomes more important.

The purpose of this investigation was to find if a currently used method of calculation of the lateral oscillation characteristics of an airplane is sufficiently accurate. This study concentrated on the short period oscillation, commonly referred to as the "Dutch roll" mode, and did not include the investigation of snaking which might appear on some aircraft. The calculated values of period and time to damp to half amplitude of the lateral oscillations (controls held fixed) were compared with experimental flight-test values to see how closely these motions could be predicted. Any discrepancies which appeared between calculated and experimental data were examined for possible causes such as aeroelasticity, unknown Mach number or altitude effects, aerodynamic lag, or incomplete derivative estimation.

It was decided to concentrate, in this investigation, on the smaller fighter-type airplanes presently flying. At the beginning of the investigation published data were not complete on most of the aircraft. Therefore, it became necessary to gather flight data from the manufacturers of the individual airplanes. In addition, wind-tunnel, geometric, and mass data for the comparable configuration were requested. The flight data used were obtained from tests conducted by the Armed Services, by the manufacturer, and by the NACA. The wind-tunnel data with the inertia and geometric characteristics were analyzed by a more or less standard calculation procedure.

The methods of calculation and the results of this survey are reported herein.

DESCRIPTION OF AIRPLANES

Geometric and mass characteristics and aerodynamic derivatives for each airplane studied are listed in table 1 for two altitudes and one Mach number. Two-view silhouettes are presented in figure 1.

The airplanes studied have jet engines. Airplanes A, D, E, F, and H are twin engined, while the rest have single engines. As can be seen in figure 1, the nine airplanes exhibit a variety of wing plan forms and fuselage shapes. Airplanes A, C, D, and E have straight wing and tail surfaces. The vertical stabilizer of airplane C has a swept-back leading edge. Airplane B has straight surfaces except for the horizontal tail, which is swept back 35°. Airplanes F, G, and H have all surfaces swept back approximately 35°. Airplane H is a semitailless design having no horizontal tail surfaces and with vertical surfaces on the wing. Airplane I has an inverse taper wing swept back 40° at the midchord line.

[redacted]

Its horizontal and vertical tail surfaces are swept back 40° and 33°, respectively. Airplanes A, B, and G have low wings; airplanes C and F have low midwings; airplanes D, H, and I have midwings; and airplane E has a high midwing. Six of the airplanes (A, C, F, G, H, and I) are single-seat fighters; B, D, and E are two-seat night or all-weather fighters.

PROCEDURE

Data Compilation

The flight data available from reports by the Armed Services and NACA were not sufficient to conduct an adequate survey. Consequently the manufacturers of each airplane were contacted to obtain the necessary information. The manufacturers were requested to furnish flight data of the type desired and information on the mass and geometric characteristics and wind-tunnel tests comparable to those of the test vehicle. The wind-tunnel test results were available in reports (some unpublished) from the NACA and other wind-tunnel facilities. The desired flight-test information was requested to be in the form of time histories of controls-fixed lateral oscillations at several altitudes over a range of speeds. These time histories were to furnish, more specifically, the period and time to damp to half amplitude of the lateral oscillations.

The manufacturers furnished flight data together with static wind-tunnel data and geometric characteristics for airplanes A, C, D, E, F, and H. Additional flight data were obtained from Armed Services reports for airplanes C and D. Wind-tunnel data and geometric characteristics were furnished for airplanes B, G, and I by the manufacturers. Flight data for airplane B came from Armed Services reports and for airplanes G and I from NACA tests.

Calculations

Appendix A presents a complete list of the symbols used in the calculations and the presentation of the data. Figure 2 shows the system of axes used for the calculations. The method of calculating the period, P, and the time to damp to half amplitude, $T_{1/2}$, is outlined in detail in appendix B. References 1 through 4 were used to estimate the rotary stability derivatives, neglecting frequency effects (reference 5). Reference 6 was used to estimate the effect of Mach number on the rotary derivatives and the low-speed static stability derivatives. The airplane was assumed to be rigid (no aeroelastic effects), and all controls were assumed fixed.

For additional methods of obtaining the lateral stability derivatives, see reference 7.

RESULTS

Comparison of the experimental and predicted values of period and time to damp to half amplitude is shown for each airplane in figures 3 through 11. The flight-test data are shown as individual points and calculated data are presented as curves. The altitudes range from 8,000 feet to 35,000 feet. It will be noted that some flight-test point symbols are filled indicating controls-fixed data. This was done only when it was definitely known by records or other means that the control surfaces were fixed. Since controls-fixed data had been requested for this investigation, they were assumed controls-fixed (indicated by the half-filled symbols) unless definitely known to be otherwise, as proven by control position records or by the method of test. If control movement was indicated, the symbols are open.

Most of the flight-test data available from the manufacturers had been gathered incidentally to other tests rather than from testing specifically for controls-fixed lateral-oscillation characteristics. As a result, the data available for some of the airplanes were rather incomplete.

No effort was made in this investigation to study snaking, a characteristic indicated by flight records of some of the airplanes at high altitudes. If the initial amplitude of the Dutch roll oscillation was large enough, the value of $T_{1/2}$ could be obtained and would be essentially independent of the snaking. Otherwise, only the period was recorded.

DISCUSSION

Based on the present and previous lateral stability investigations, it appears that ability to predict controls-fixed period, P, and damping, $1/T_{1/2}$, to within about ±20 percent is sufficiently accurate to be useful in the design of tactical aircraft. Consequently, this figure will be used to distinguish between satisfactory and unsatisfactory results in the following presentation.

Several factors determined this choice. It is doubtful that current or future flying-qualities requirements involving lateral-oscillation period and damping can define satisfactory and unsatisfactory behavior to any greater accuracy than ±20 percent. Experience has indicated

[redacted]

(see reference 8, for example) that pilots generally do not discern or react to changes in period and damping of much less than ±20 percent. Scatter in flight data can be attributed to small variations in speed and altitude, recording inaccuracies, and errors or generalizations involved in data reduction. It has been found that this scatter can be held below ±20 percent only in a carefully performed experiment.

In figures 12 and 13 are plotted the values of measured period and damping (reciprocal of time to damp to half amplitude) against the predicted values for each of the airplanes. Also shown on these plots are the lines of perfect agreement and ±20 percent disagreement. Generally, it may be seen in figure 12 that the period could be predicted with reasonable accuracy. In figure 13, it may be noted that with the exception of airplanes B, E, and I, the prediction of damping was satisfactory. The reasons for the poor correlation for these three airplanes will be discussed later.

Airplane A

It may be seen in figure 3 that for this airplane the correlation between experimental and predicted period at 10,000 feet altitude and time to damp to half amplitude at 10,000 and 30,000 feet is good. The comparison of experimental and predicted period at 30,000 feet altitude, however, shows poor agreement. A general increase of the predicted curve by 30 percent would bring about good correlation. It is not known what caused this disparity between the measured and predicted data at 30,000 feet altitude. Comparison with the data of the other airplanes included herein of similar configuration shows that the measured period of airplane A increases by 70 to 80 percent in going from 10,000 to 30,000 feet altitude; while the measured values of period for the other airplanes increase by only 40 to 50 percent. This fact might cause doubt of the accuracy of the measured data except that the measured data available appear to be repeatable. There is the possibility that a moving free rudder could be the cause of the increase in period.

Airplane B

The data available for airplane B were too sparse to provide a ready means of comparison between the predicted and measured values of period and damping. Figures 12 and 13 indicate good agreement among the values of period but poor correlation among the damping values. It will also be noted (see fig. 4) that the damping decreases markedly in the low Mach number range.

[redacted]

At the time the calculations were made, wind-tunnel sideslip data were not available for the complete airplane configuration tested in flight. An increase of wing geometric dihedral to 7.0° for airplane B, as compared with 3.6° for the preceding airplane of the series (for which low-speed wind-tunnel sideslip data were available), accompanied by a reduction in wing thickness, required that corrections be made to dihedral effect, C_{l_β}. The low-speed values of C_{n_β} and C_{Y_β} were taken directly from the wind-tunnel data available and all rotary derivatives were computed by the methods of appendix B.

The high dihedral effect of this airplane is the main cause of the low damping present and is partly responsible for the poor correlation between the predicted and measured damping.

Airplane C

The correlation for the period and the damping is good at the 10,000-foot altitude (fig. 5). Predicted and experimental values of damping do not agree well at 30,000 feet. The measured values show better damping than predicted. The scatter in the data is a little larger than usual, which could cause some of the discrepancy.

Airplane D

The data available for airplane D indicated good correlation (see figs. 6, 12, and 13). The test data for damping at 30,000 feet (not shown) indicated considerable scatter and were considered unreliable for comparison. Most of the flight-test data were obtained with the stick held fixed but with the rudder free. Small oscillations of the rudder which were present could possibly be responsible for the slightly higher experimental times to damp to half amplitude as compared with predicted values. The necessity of actually having the rudder locked during flight tests cannot be overstressed since even small oscillations in proper phase allowed by cable stretch from locked controls can change the damping considerably (see reference 9, for example).

Airplane E

The correlation of predicted and measured period of airplane E is generally satisfactory (figs. 7, 12, and 13). The damping correlation is not satisfactory. Figure 7 shows variations in the experimental data which accompanied the noted changes in configuration during the

flight-test program. This airplane, as tested, was subject to snaking oscillations so that some of the flight data for damping were unsatisfactory for comparison.

The desirability of obtaining more extensive dynamic wind-tunnel data was demonstrated in the development testing of airplane E. When the early flight tests indicated that the damping was lower than predicted, a model was placed in the tunnel by the manufacturer for further tests. This model was spindle mounted, permitting it to be oscillated in yaw. Tests of this arrangement also gave less damping than predicted from static wind-tunnel tests. Wake surveys subsequently made in the region of the tail showed that the fuselage was acting as a lifting surface in yaw, with vortices from the fuselage trailing near the tail. The high position of the vertical tail, however, placed it only in the upper part of this vortex flow, which is destabilizing, that is, it fortifies the side flow in the direction in which the tail is moving. The destabilizing effect of the vortices could be reduced by use of a lower vertical tail position, an expensive problem in redesign after an airplane is built.

The above change in damping would be more properly termed $C_{n_{\dot{\beta}}}$ than a change in C_{n_r} (see symbols, appendix A). In that case, the total damping-in-yaw derivative should include the effects of both C_{n_r} and $C_{n_{\dot{\beta}}}$. In the calculations for airplane E, the results of which are shown in figure 7, C_{n_r} was modified to include the approximate effect of $C_{n_{\dot{\beta}}}$ as indicated in appendix B. This modification increased the predicted values of time to damp to half amplitude by 38 to 89 percent. Plotted in figure 7 are curves of time to damp to half amplitude with C_{n_r} modified and C_{n_r} unmodified (dashed line) for one altitude (8,000 feet).

It would appear then that care in estimating the rotary damping in yaw must be exercised if accurate values are to be computed, especially if the static wind-tunnel tests indicate the presence of large sidewash variations at the vertical tail.

Airplane F

The majority of the flight-test points available for airplane F (fig. 8) were at 10,000 feet altitude. These indicate a slightly shorter period and slightly longer time to damp to half amplitude than the calculated values. Generally, there is good agreement between predicted and measured values of period and damping for the three altitudes shown (see figs. 12 and 13). Some of the flight-test points for damping were not plotted due to incomplete or too short time histories available.

[redacted]

Airplane G

Airplane G shows very good correlation between predicted and measured values of period (see fig. 12). Generally, the correlation of damping is good (fig. 13) with a few points falling outside the ±20 percent boundaries. It may be seen in figure 9 that most of these points are at the limits of the scatter present. A more complete description of the correlation between predicted and measured lateral stability characteristics for airplane G may be found in reference 10.

Airplane H

The six experimental test points available for airplane H (fig. 10) indicate fairly good agreement between the predicted and measured values of period and damping. These few flight-test points, however, are too sparse to provide a definite comparison.

Airplane I

Reference to figure 11 shows, for airplane I, marginal agreement between measured and calculated values of period. The prediction of time to damp to half amplitude is poor. Predicted values of the period are somewhat lower than the flight results over the entire Mach number range for the altitudes of 10,000, 20,000, and 30,000 feet, with a maximum disagreement of −20 percent. The predicted variation of $T_{1/2}$ with Mach number is generally in poor agreement with experimental results, and shows an over-all decrease with increasing Mach number much greater than is shown from flight tests. At 20,000 and 30,000 feet, the agreement between measured and calculated damping is very poor, particularly in the low Mach number range tested at each altitude. At 30,000 feet, for example, at a Mach number of 0.55, the calculated value of $T_{1/2}$ is approximately 100 percent greater than the experimental value. Because of the unusual configuration of this airplane (swept, inverse-tapered wing, and short tail length), it is likely that present methods of computing the rotary derivatives (C_{n_p}, C_{n_r}, etc.) from static wind-tunnel data and geometric characteristics are not applicable. Period and time to damp to half amplitude were recomputed for the range of Mach numbers considered at 10,000 feet, neglecting C_{n_p}. The results of these calculations are presented in figure 11 and show good agreement between predicted and experimental damping at the lower Mach numbers, indicating that C_{n_p} may be much smaller in magnitude throughout the lift coefficient range than was computed. Direct measurement of the rotary derivatives in curved- and rolling-flow stability tunnels would probably

furnish data more reliable for use in calculating the damping of this airplane.

CONCLUDING REMARKS

Where a sufficient (enough to show repeatability) number of good flight-test points were available, the correlation of predicted and measured lateral-oscillation characteristics was usually satisfactory for the smaller fighter-type jet airplanes investigated. In all cases studied, the order of magnitude of the damping could be predicted. In general, the prediction accuracy with regard to the damping was much greater for well-damped airplanes, indicating the error may be a given uncertainty rather than a given percentage.

A configuration with which the designer is familiar, such as one having only slight changes from previous airplanes, may have its lateral characteristics calculated fairly accurately by this method. However, a radical change in a model or a new configuration makes more extensive wind-tunnel tests highly desirable and in many cases necessary. These tests should include at least determination of C_{n_r} and $C_{n_{\dot{\beta}}}$ as well as the usual static data. Good experimental values of the other rotary derivatives are also desirable.

Ames Aeronautical Laboratory
National Advisory Committee for Aeronautics
Moffett Field, Calif.

[redacted]

APPENDIX A

SYMBOLS

The stability system of axes used in this investigation is defined as an orthogonal system having its origin at the center of gravity and in which the X axis extends along the flight path, the Z axis is in the plane of symmetry and perpendicular to the X axis, and the Y axis is perpendicular to the plane of symmetry. See figure 2.

b	wing span, feet
i_w	wing incidence, degrees
l	distance of center of pressure of vertical tail aft of the Z axis, feet
m	mass, slugs
p	rolling angular velocity about the X axis, radians per second
q	dynamic pressure $\left(\frac{1}{2}\rho V^2\right)$, pounds per square foot
r	yawing angular velocity about the Z axis, radians per second
t	time, seconds
z	distance of center of pressure of vertical tail from X axis, positive when center of pressure is above X axis, feet
L	rolling moment about X axis, foot-pounds
M	Mach number
N	yawing moment about Z axis, foot-pounds
P	period, seconds
S	wing area, square feet
$T_{1/2}$	time for amplitude of oscillation to decrease by one-half, seconds
V	velocity, feet per second
W	weight, pounds
Y	lateral force along Y axis, pounds

[redacted]

α angle of attack of fuselage reference line, degrees

β angle of sideslip, radians

γ angle between flight path and horizontal, degrees

ϵ angle between reference axis and principal longitudinal axis, positive when the reference axis is above the principal axis at the nose, degrees

η inclination of the principal longitudinal axis of the airplane with respect to the flight path, positive when the principal axis is above the flight path at the nose, degrees

μ relative density factor $\left(\frac{m}{\rho S b}\right)$

ρ mass density of air, slugs per cubic foot

σ sidewash angle, positive for positive side force, radians

φ angle of bank, radians

Ψ angle of yaw, radians

C_L lift coefficient $\left(\frac{\text{lift}}{qS}\right)$

C_l rolling-moment coefficient $\left(\frac{L}{qSb}\right)$

C_n yawing-moment coefficient $\left(\frac{N}{qSb}\right)$

C_Y lateral-force coefficient $\left(\frac{Y}{qS}\right)$

C_{l_β} $\frac{\partial C_l}{\partial \beta}$

C_{n_β} $\frac{\partial C_n}{\partial \beta}$

$C_{n_{\dot{\beta}}}$ $\frac{\partial C_n}{\partial (d\beta/dt)}$

C_{Y_β} $\frac{\partial C_Y}{\partial \beta}$

[redacted]

C_{l_p} $\dfrac{\partial C_l}{\partial(pb/2V)}$

C_{n_p} $\dfrac{\partial C_n}{\partial(pb/2V)}$

C_{Y_p} $\dfrac{\partial C_Y}{\partial(pb/2V)}$

C_{l_r} $\dfrac{\partial C_l}{\partial(rb/2V)}$

C_{n_r} $\dfrac{\partial C_n}{\partial(rb/2V)}$

C_{Y_r} $\dfrac{\partial C_Y}{\partial(rb/2V)}$

k_{x_o} radius of gyration in roll about principal longitudinal axis, feet

k_{z_o} radius of gyration in yaw about principal vertical axis, feet

K_{x_o} $\dfrac{k_{x_o}}{b}$

K_{z_o} $\dfrac{k_{z_o}}{b}$

K_x nondimensional radius of gyration about longitudinal stability axis $\left(\sqrt{K_{x_o}^2 \cos^2 \eta + K_{z_o}^2 \sin^2 \eta}\right)$

K_z nondimensional radius of gyration about vertical stability axis $\left(\sqrt{K_{z_o}^2 \cos^2 \eta + K_{x_o}^2 \sin^2 \eta}\right)$

K_{xz} nondimensional product-of-inertia parameter $\left[(K_{z_o}^2 - K_{x_o}^2) \cos \eta \sin \eta\right]$

[redacted]

APPENDIX B

CALCULATION METHODS

In making the calculations of this investigation, the airplane was treated as a rigid body and values of period and damping were found by use of the following three linearized nondimensional equations of lateral motion referred to the stability system of axes:

Roll

$$\left(2\mu K_x^2 D^2 - \frac{1}{2}\frac{V}{b} C_{l_p} D\right)\varphi + \left(2\mu K_{xz} D^2 - \frac{1}{2}\frac{V}{b} C_{l_r} D\right)\psi - \left(\frac{V}{b}\right)^2 C_{l_\beta}\beta = 0$$

Yaw

$$\left(2\mu K_{xz} D^2 - \frac{1}{2}\frac{V}{b} C_{n_p} D\right)\varphi + \left(2\mu K_z^2 D^2 - \frac{1}{2}\frac{V}{b} C_{n_r} D\right)\psi - \left(\frac{V}{b}\right)^2 C_{n_\beta}\beta = 0$$

Sideforce

$$\left(-\frac{1}{2} C_{Y_p} D - \frac{V}{b} C_L\right)\varphi + \left[\left(2\mu - \frac{1}{2} C_{Y_r}\right) D - \frac{V}{b} C_L \tan\gamma\right]\psi + \left(2\mu D - \frac{V}{b} C_{Y_\beta}\right)\beta = 0$$

where

$$D = \frac{d}{dt}$$

By use of these equations the stability quartic was obtained. This was solved by synthetic division to obtain values of the period and time to damp to half amplitude as follows:

$$P = \frac{2\pi}{b} \qquad T_{1/2} = \frac{-0.693}{a}$$

where a and b are the real and imaginary parts of the complex roots, respectively. The data to ascertain the coefficients of these equations were supplied partially by the manufacturers concerned and partially by normal methods of computation from basic data. The weight and mass data were obtained from the manufacturers together with values of the static lateral stability derivatives (C_{l_β}, C_{n_β}, C_{Y_β}) which had come from wind-tunnel tests of the model most closely representing the airplane

[redacted]

upon which flight tests were made. The rotary or dynamic derivatives were obtained by NACA methods of calculation (outlined herein) using the static derivatives and the airplane geometric characteristics as a base. The derivatives could be approximated by considering the geometric theory alone, but the results of wind-tunnel tests provide more accurate data to use. Recent wind-tunnel tests using rotary balances or curved or rolling flow have been successful in providing empirical data useful for specific configurations.

For these calculations no attempt was made to include a fuselage effect. It is usually considered negligible for conventional airplanes. Therefore, the contributions of the wing and the vertical and horizontal tails to the various derivatives were obtained and then algebraically added. Generally, the equations of reference 1 modified for Mach number effects by the methods of reference 6 were found to give reasonable results for the wing contribution.

Damping in Roll, C_{l_p}

The values of both the wing and horizontal tail contributions to C_{l_p} were obtained by the methods of reference 2. The charts presented in that reference provided a rapid means of estimation for wide ranges of aspect ratios, taper ratios, and positive and negative sweep angles.

The vertical tail contribution to C_{l_p} as well as C_{n_p} and C_{Y_p} was estimated by the equations presented in reference 4 as follows:

$$C_{l_{p_t}} = C_{Y_{\beta_t}} \left(\frac{z}{b} \cos \alpha - \frac{l}{b} \sin \alpha \right) \left[2 \left(\frac{z}{b} \cos \alpha - \frac{l}{b} \sin \alpha \right) - \frac{\partial \sigma}{\partial (pb/2V)} \right]$$

In this equation, $\partial\sigma/\partial(pb/2V)$ is termed the "sidewash factor." Values of this factor found to apply over a moderate range of angles of attack and for wings with and without sweep and a further discussion may be found in reference 3. Generally, it was found that the introduction of this sidewash factor served to reduce the vertical tail contribution so that C_{l_p} for the total airplane could be approximated by the value of C_{l_p} for the wing alone. Values of $C_{Y_{\beta_t}}$ in this and the following equations were obtained from wind-tunnel data.

Yawing Moment Due to Rolling, C_{n_p}

The contribution of the wing to C_{n_p} was determined by the methods of reference 1. These values were further corrected for Mach number effects by equation (3) of reference 6. The horizontal tail contribution was considered negligible. The vertical tail contribution was determined by the following equation from reference 4:

$$C_{n_{p_t}} = -C_{Y_{\beta_t}}\left(\frac{z}{b}\sin\alpha + \frac{l}{b}\cos\alpha\right)\left[2\left(\frac{z}{b}\cos\alpha - \frac{l}{b}\sin\alpha\right) - \frac{\partial\sigma}{\partial(pb/2V)}\right]$$

Side Force Due to Rolling, C_{Y_p}

The side force due to roll of the wing is dependent upon the sweep. Straight wings are assumed to have no, or negligible, side force due to roll. Swept wings do contribute a value to this derivative. Values for the wing were obtained from the methods of references 1 and 6; the horizontal tail was neglected. The following equation of reference 4 was used to estimate C_{Y_p} due to the vertical tail:

$$C_{Y_{p_t}} = C_{Y_{\beta_t}}\left[2\left(\frac{z}{b}\cos\alpha - \frac{l}{b}\sin\alpha\right) - \frac{\partial\sigma}{\partial(pb/2V)}\right]$$

In the calculations for several of the airplanes included herein, values of C_{Y_p} and C_{Y_r} were not calculated or used since they have a negligible effect on the period and damping.

Rolling Moment Due to Yawing, C_{l_r}

The horizontal tail was neglected in obtaining the yawing dynamic derivatives. The contribution of the wing to C_{l_r} was obtained by means of references 1 and 6. The vertical tail contribution was obtained by the following formula (reference 11):

$$C_{l_{r_t}} = -2\frac{l}{b}\left(\frac{z}{b} - \frac{l}{b}\sin\alpha\right)C_{Y_{\beta_t}}$$

[redacted]

Damping in Yaw, C_{n_r}

No Mach number correction was applied to the values of C_{n_r} for the wing as obtained from reference 1. The vertical tail contribution to C_{n_r} was obtained by the following formula (reference 11):

$$C_{n_{r_t}} = 2\left(\frac{l}{b}\right)^2 C_{Y_{\beta_t}}$$

As noted in the discussion, the damping of airplane E was found to be less than that calculated by use of static wind-tunnel data. Consequently, for the study of this airplane, the calculated value of C_{n_r} for the total airplane, at a given Mach number and C_L, was reduced in magnitude by an amount equal to the difference between $C_{n_{r_t}}$ as calculated and $C_{n_{r_t}}$ as obtained in the wind-tunnel tests of the spindle-mounted model of airplane E. The difference between $C_{n_{r_t}}$ as calculated and as measured in the wind tunnel is approximately equal to C_{n_β}. These modified values of C_{n_r} were used to obtain the predicted curves of figure 7.

Side Force Due to Yawing, C_{Y_r}

The wing contribution to C_{Y_r} was obtained by the method of reference 1 with no Mach number correction. Vertical tail values of C_{Y_r} (reference 11) were obtained by:

$$C_{Y_{r_t}} = -2\,\frac{l}{b}\,C_{Y_{\beta_t}}$$

It should be noted that the success of these calculations in producing good values of the rotary derivatives is dependent upon accurate static wind-tunnel data.

[redacted]

REFERENCES

1. Toll, Thomas A., and Queijo, M. J.: Approximate Relations and Charts for Low-Speed Stability Derivatives of Swept Wings. NACA TN 1581, 1948.

2. DeYoung, John: Theoretical Antisymmetric Span Loading for Wings of Arbitrary Plan Form at Subsonic Speeds. NACA TN 2140, 1950.

3. Michael, William H., Jr: Analysis of the Effects of Wing Interference on the Tail Contributions to the Rolling Derivatives. NACA TN 2332, 1951.

4. Letko, William, and Riley, Donald R.: Effect of an Unswept Wing on the Contribution of Unswept-Tail Configurations to the Low-Speed Static- and Rolling-Stability Derivatives of a Midwing Airplane Model. NACA TN 2175, 1950.

5. Bird, John D., Fisher, Lewis R., and Hubbard, Sadie M.: Some Effects of Frequency on the Contribution of a Vertical Tail to the Free Aerodynamic Damping of a Model Oscillating in Yaw. NACA TN 2657, 1952.

6. Fisher, Lewis R.: Approximate Corrections for the Effects of Compressibility on the Subsonic Stability Derivatives of Swept Wings. NACA TN 1854, 1949.

7. Campbell, John P., and McKinney, Marion O.: Summary of Methods for Calculating Dynamic Lateral Stability and Response and for Estimating Lateral Stability Derivatives. NACA TN 2409, 1951.

8. Liddell, Charles J., Jr., Creer, Brent Y., and Van Dyke, Rudolph D., Jr.: A Flight Study of Requirements for Satisfactory Lateral Oscillatory Characteristics of Fighter Aircraft. NACA RM A51E16, 1951.

9. Stough, Carl J., and Kauffman, William M.: A Flight Investigation and Analysis of the Lateral-Oscillation Characteristics of an Airplane. NACA TN 2195, 1950.

10. McNeill, Walter E., and Cooper, George E.: A Comparison of the Measured and Predicted Lateral Oscillatory Characteristics of a 35° Swept-Wing Fighter Airplane. NACA RM A51C28, 1951.

[redacted]

11. Letko, William: Effect of Vertical-Tail Area and Length on the Yawing Stability Characteristics of a Model Having a 45° Swept Back Wing. NACA TN 2358, 1951.

[redacted]

TABLE I.- PARAMETERS USED IN CALCULATIONS FOR AIRPLANES INVESTIGATED AT TWO ALTITUDES AND ONE MACH NUMBER [M = 0.50]

Airplane	A		B		C		D		E		F		G		H		I	
Altitude, ft	10,000	30,000	10,000	30,000	10,000	30,000	10,000	30,000	8,000	30,000	10,000	30,000	10,000	35,000	10,000	30,000	10,000	30,000
W	15,000	14,000	15,276	15,276	13,000	13,000	18,100	18,100	31,000	31,000	16,995	16,995	12,500	12,500	18,900	17,200	19,535	19,535
b	41.62	41.62	37.63	37.63	35.25	35.25	50.00	50.00	52.00	52.00	39.66	39.66	37.12	37.12	38.67	38.67	31.23	31.23
S	294.09	294.09	252.80	252.80	250.00	250.00	400.00	400.00	606.00	606.00	350.00	350.00	287.90	287.90	496.00	496.00	380.00	380.00
W/S	51.0	47.6	65.6	65.6	52.0	52.0	45.2	45.2	51.1	51.1	48.5	48.5	43.4	43.4	38.1	34.7	61.0	61.0
m	466.0	434.5	474.9	474.9	404.1	404.1	562.1	562.1	963.63	963.63	528.3	528.3	388.5	388.5	587.5	534.7	607.24	607.24
μ	21.674	39.958	15.983	11.099	26.114	51.581	16.005	31.615	16.362	34.398	21.672	42.808	20.702	49.393	17.443	31.358	34.609	68.349
C_L	0.200	0.433	0.258	0.386	0.204	0.473	0.178	0.412	0.186	0.469	0.187	0.443	0.171	0.499	0.150	0.322	0.242	0.556
α	1.58	4.00	1.37	2.64	2.44	5.06	-2.45	0.35	2.54	6.21	2.55	5.91	1.97	6.51	2.54	5.45	2.95	8.15
i_w	0	0	0	0	0	0	4.09	4.09	1.5	1.5	1.00	1.00	root + 1 tip - 1	root + 1 tip - 1	0	0	0	0
η	-2.37	0.05	0.14	1.41	-1.51	1.11	-4.50	-1.70	-2.76	0.91	-0.90	2.46	-0.53	4.01	1.67	4.58	1.45	6.65
ϵ	3.95	3.95	1.23	1.23	3.95	3.95	2.05	2.05	5.30	5.30	3.45	3.45	2.50	2.50	0.87	0.87	1.50	1.50
K_x^2	0.01551	0.01547	0.01808	0.01811	0.01529	0.01528	0.01146	0.01132	0.03860	0.03855	0.01382	0.01378	0.01353	0.01367	0.02804	0.02680	0.02508	0.02583
K_z^2	0.04083	0.04087	0.07098	0.07095	0.04978	0.04979	0.03830	0.03844	0.05819	0.05824	0.07522	0.07512	0.04332	0.04318	0.06635	0.06503	0.06866	0.06784
K_{xz}	-0.00105	0.00002	0.00013	0.00130	-0.00091	0.00067	-0.00213	-0.00081	-0.00124	0.00041	-0.00097	0.00866	-0.00028	0.00208	0.00112	0.00313	0.00161	0.00733
C_{l_p}	-0.4498	-0.4480	-0.430	-0.429	-0.466	-0.464	-0.478	-0.476	-0.374	-0.372	-0.3539	-0.3453	-0.358	-0.357	-0.284	-0.297	-0.314	-0.288
C_{l_r}	0.0680	0.1250	0.107	0.125	0.098	0.154	0.084	0.140	0.072	0.139	0.1100	0.1562	0.090	0.157	0.054	0.093	0.180	0.244
C_{n_p}	0.0143	-0.0017	-0.046	-0.056	-0.002	-0.021	-0.001	-0.020	-0.006	-0.023	0.0138	-0.0235	-0.013	-0.045	0.026	0.016	-0.036	-0.081
C_{n_r}	-0.1186	-0.1155	-0.201	-0.202	-0.153	-0.157	-0.136	-0.138	-0.058	-0.077	-0.3299	-0.3405	-0.182	-0.183	-0.087	-0.089	-0.342	-0.329
C_{Y_p}	-0.0628	-0.0561	- - -	- - -	-0.016	0.001	-0.016	0.009	-0.004	0.008	-0.0180	0.1450	- - -	- - -	- - -	- - -	- - -	- - -
C_{Y_r}	0.2663	0.2680	- - -	- - -	0.376	0.376	0.373	0.373	0.188	0.194	0.4970	0.4830	- - -	- - -	- - -	- - -	- - -	- - -
C_{Y_β}	-0.5300	-0.5370	-0.690	-0.690	-0.619	-0.619	-0.638	-0.638	-0.348	-0.362	-0.5730	-0.5730	-0.673	-0.690	-0.590	-0.595	-0.840	-0.765
C_{n_β}	0.1680	0.1670	0.116	0.116	0.124	0.124	0.101	0.109	0.063	0.069	0.1811	0.1866	0.103	0.110	0.114	0.110	0.193	0.171
C_{l_β}	-0.0735	-0.0735	-0.107	-0.105	-0.110	-0.110	-0.078	-0.078	-0.040	-0.046	-0.0613	-0.0728	-0.064	-0.102	-0.024	-0.036	-0.170	-0.210

NACA

[redacted]

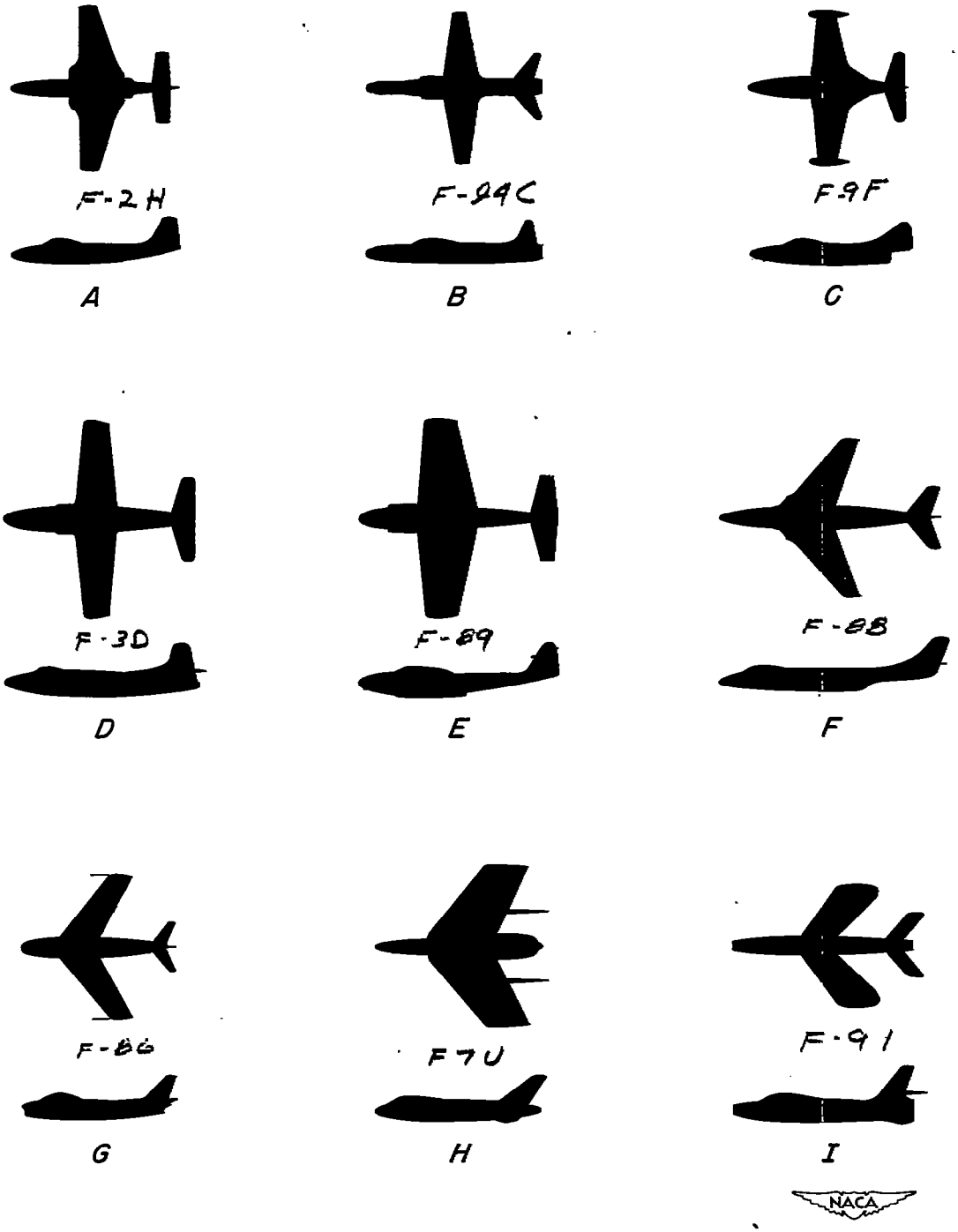

Figure I.- Two-view silhouettes of the nine airplanes investigated.

[redacted]

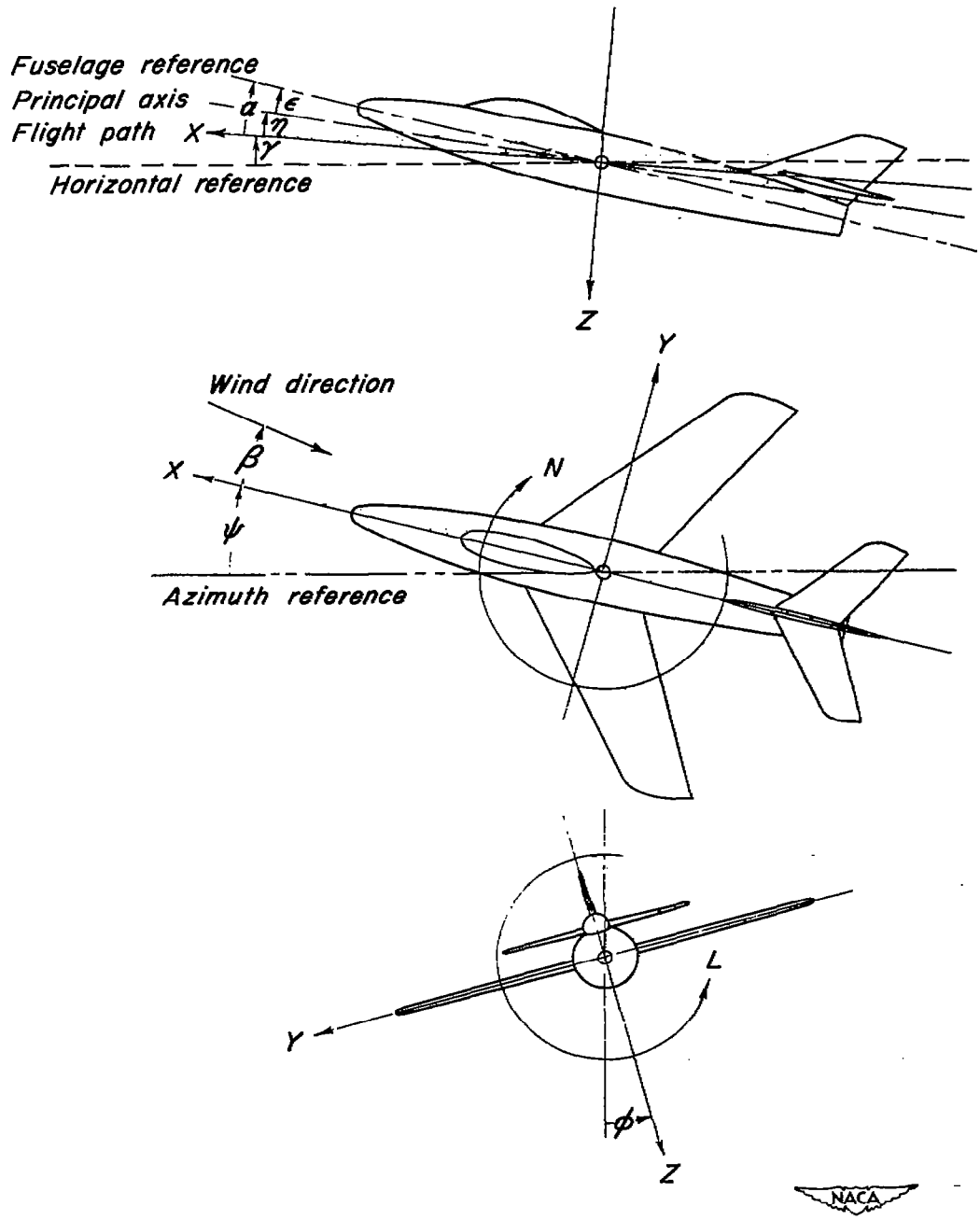

Figure 2.—System of axes and angles used in calculations. Arrows indicate positive values of forces, moments, and angles.

[redacted]

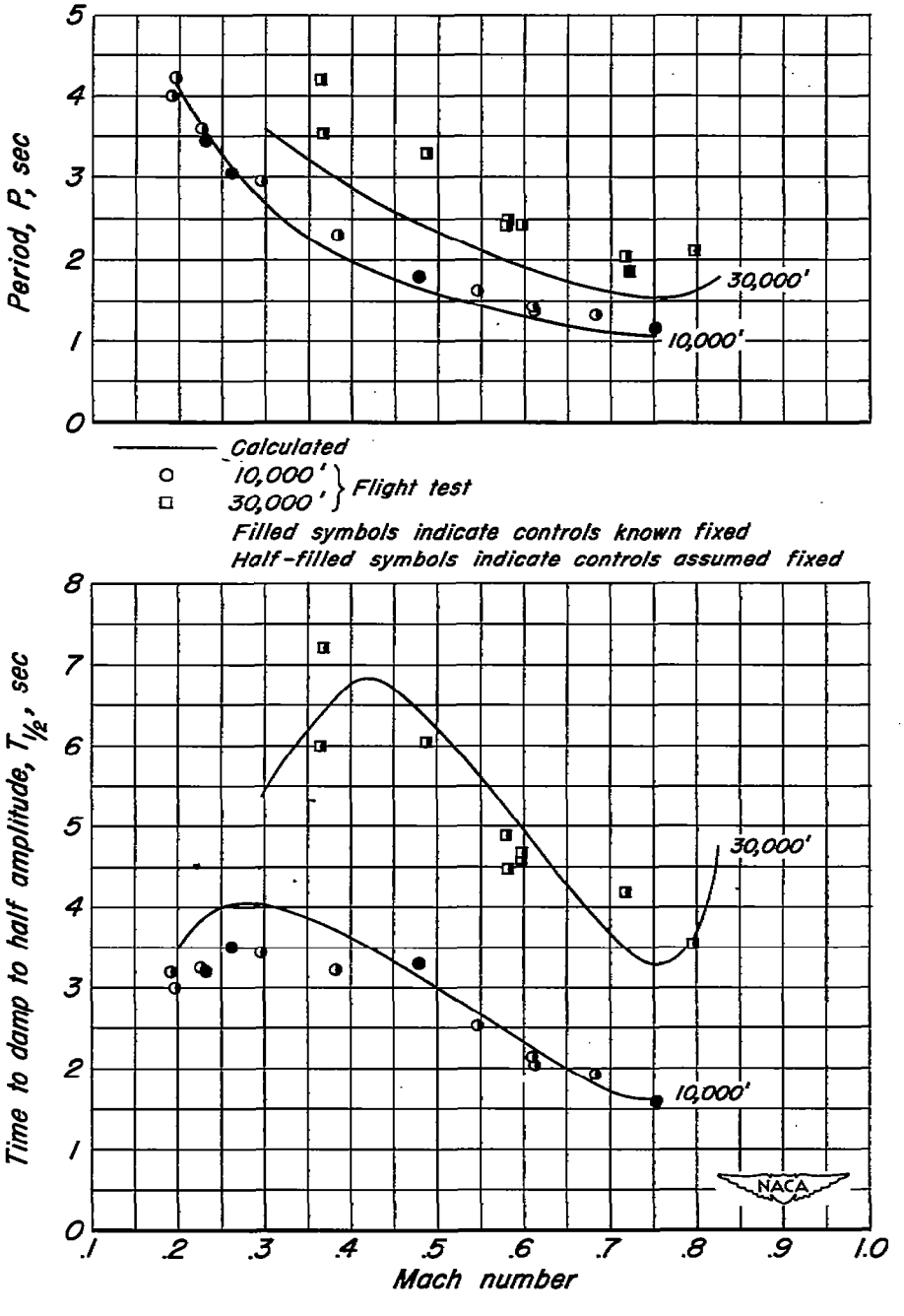

Figure 3.– Variation of period and time to damp to half amplitude with Mach number for airplane A.

[redacted]

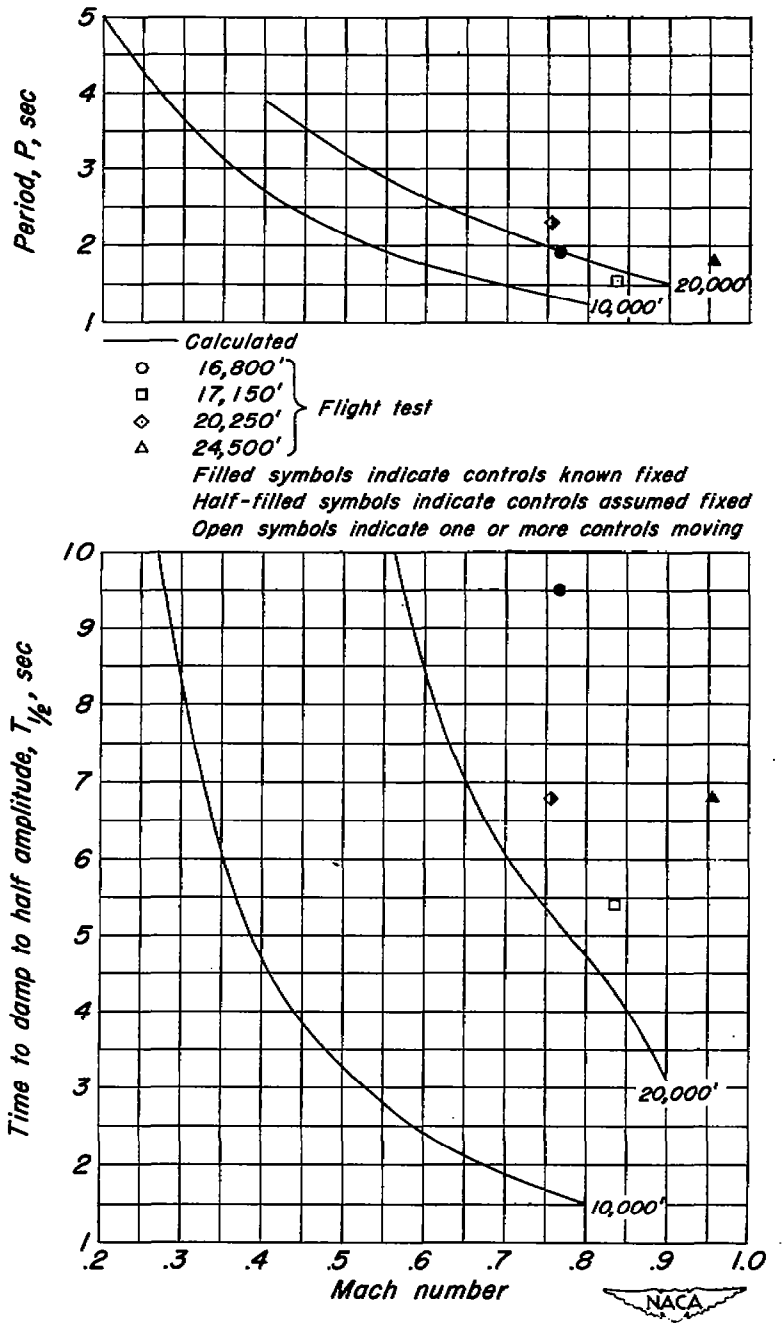

Figure 4.–Variation of period and time to damp to half amplitude with Mach number for airplane B.

[redacted]

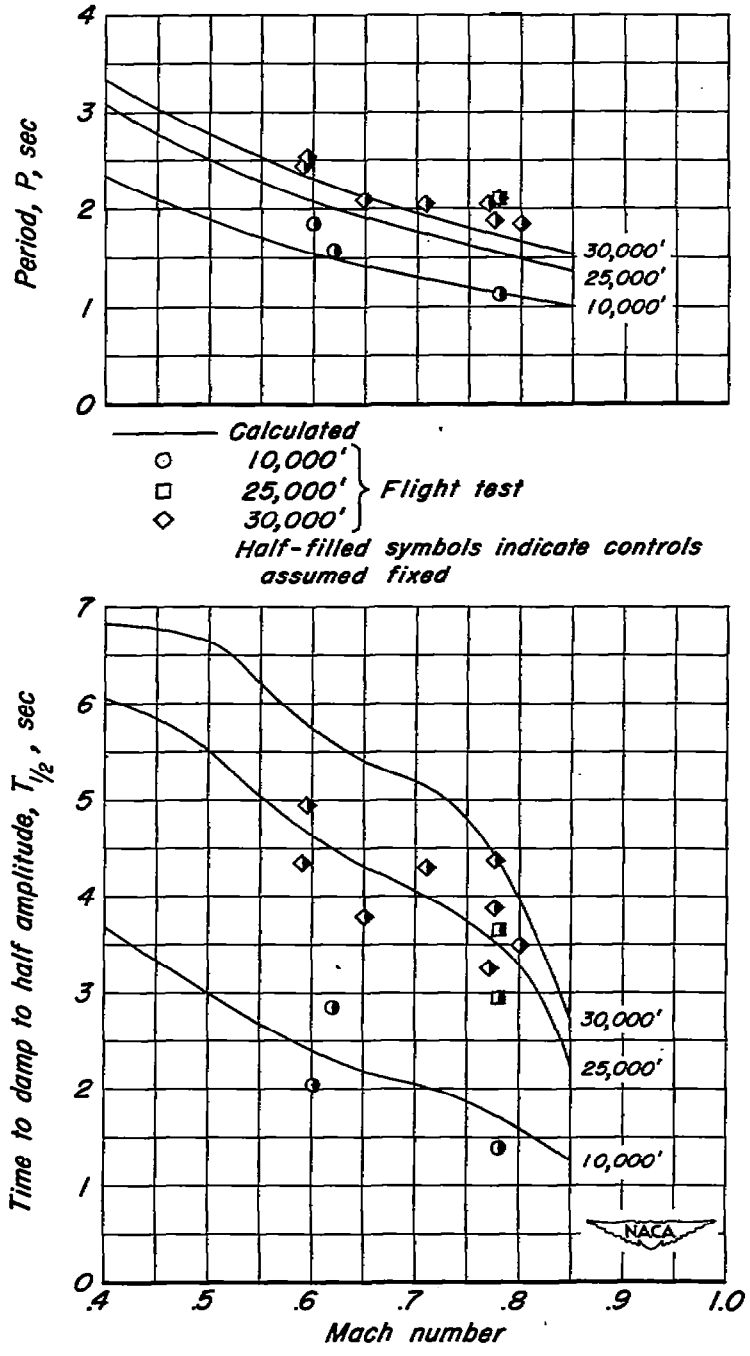

Figure 5.- Variation of period and time to damp to half amplitude with Mach number for airplane C.

[redacted]

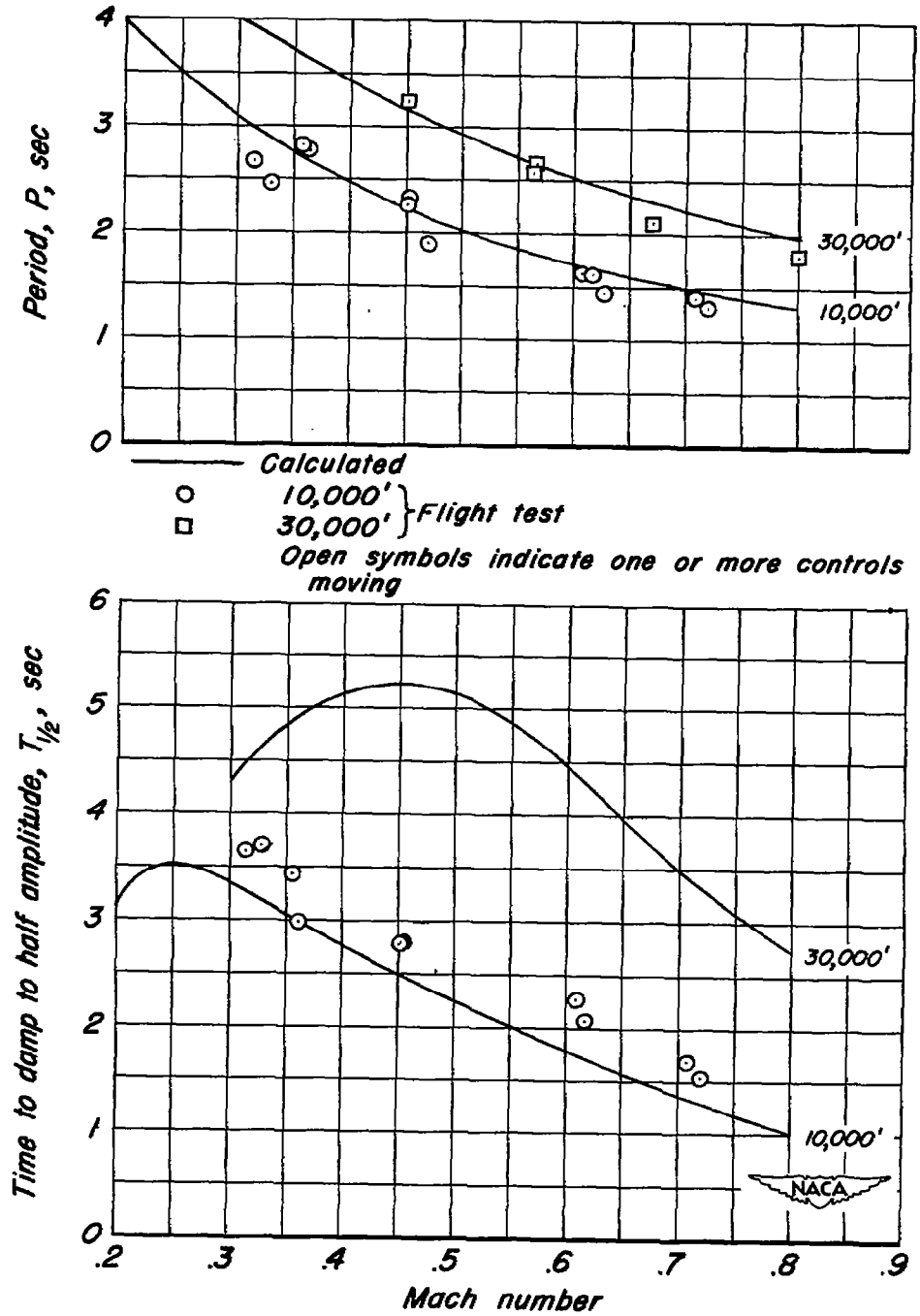

Figure 6.- Variation of period and time to damp to half amplitude with Mach number for airplane D.

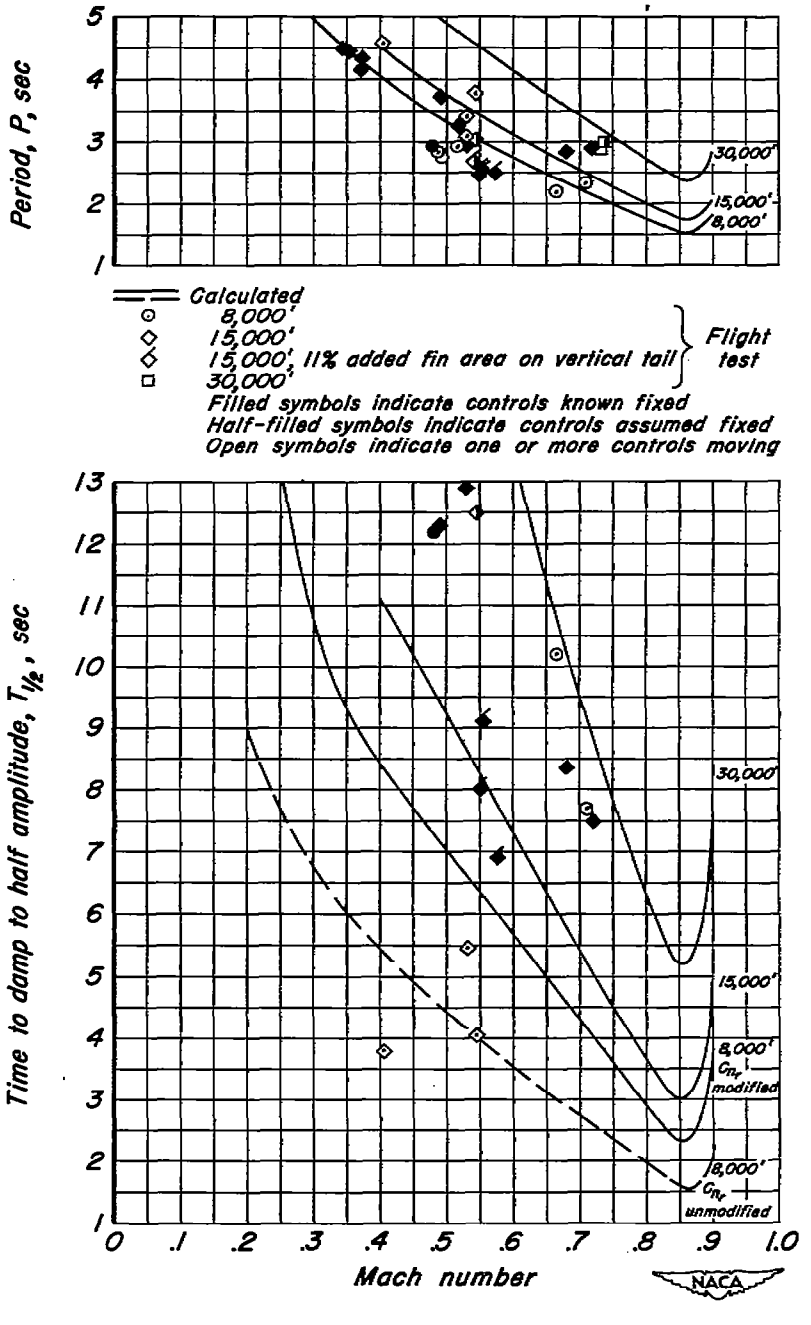

Figure 7.- Variation of period and time to damp to half amplitude with Mach number for airplane E.

[redacted]

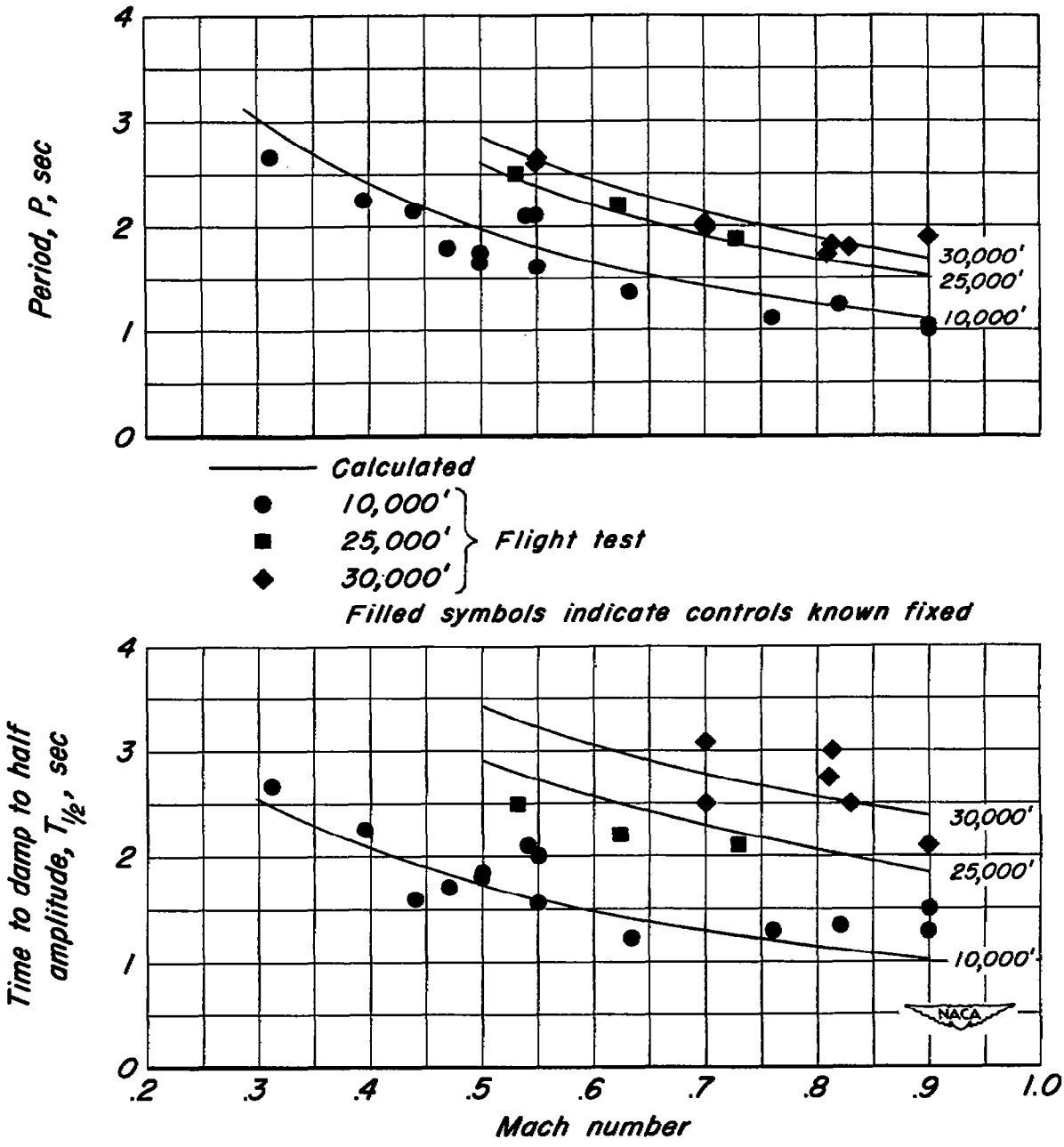

Figure 8.- Variation of period and time to damp to half amplitude with Mach number for airplane F.

[redacted]

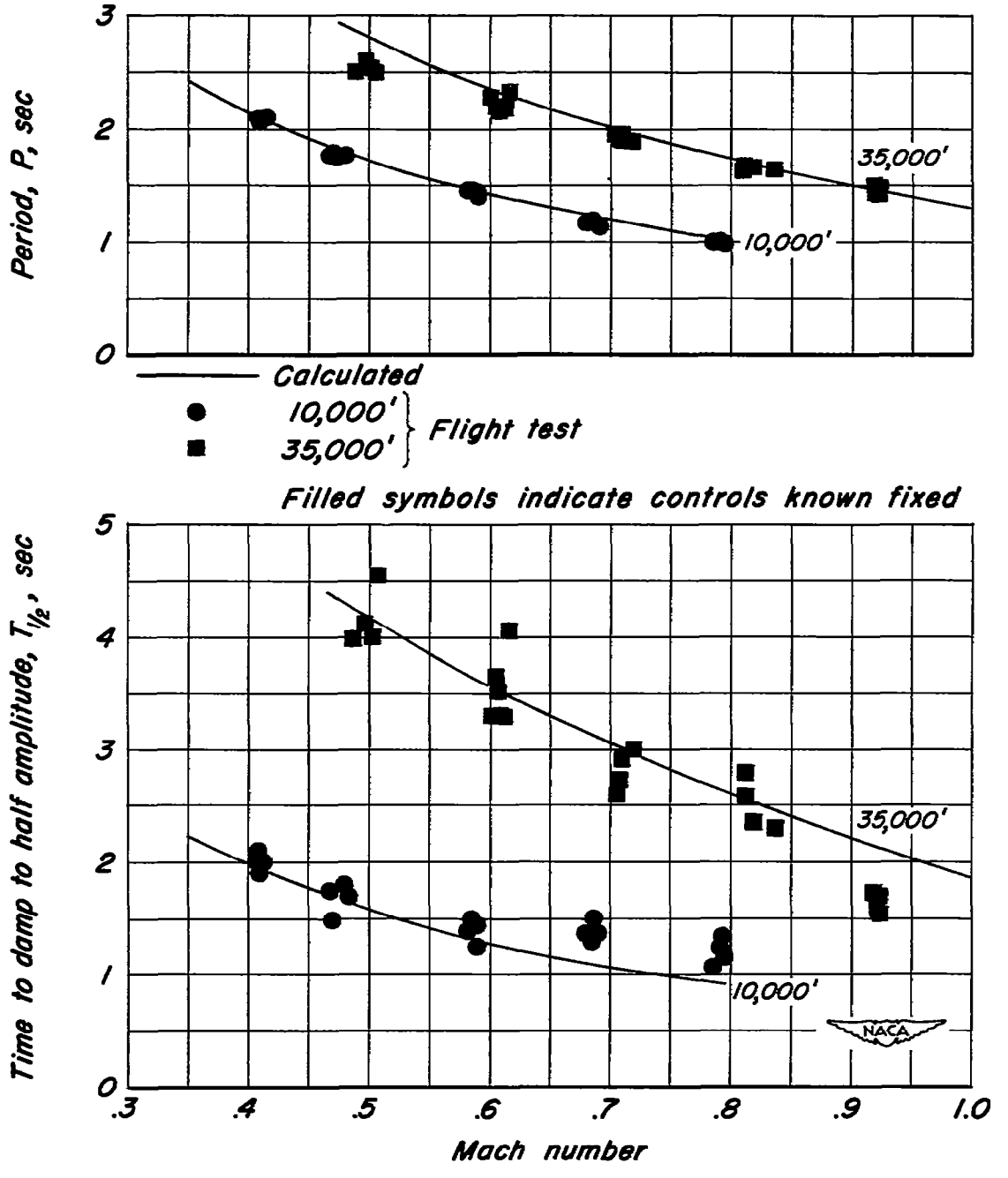

Figure 9.- Variation of period and time to damp to half amplitude with Mach number for airplane G.

[redacted]

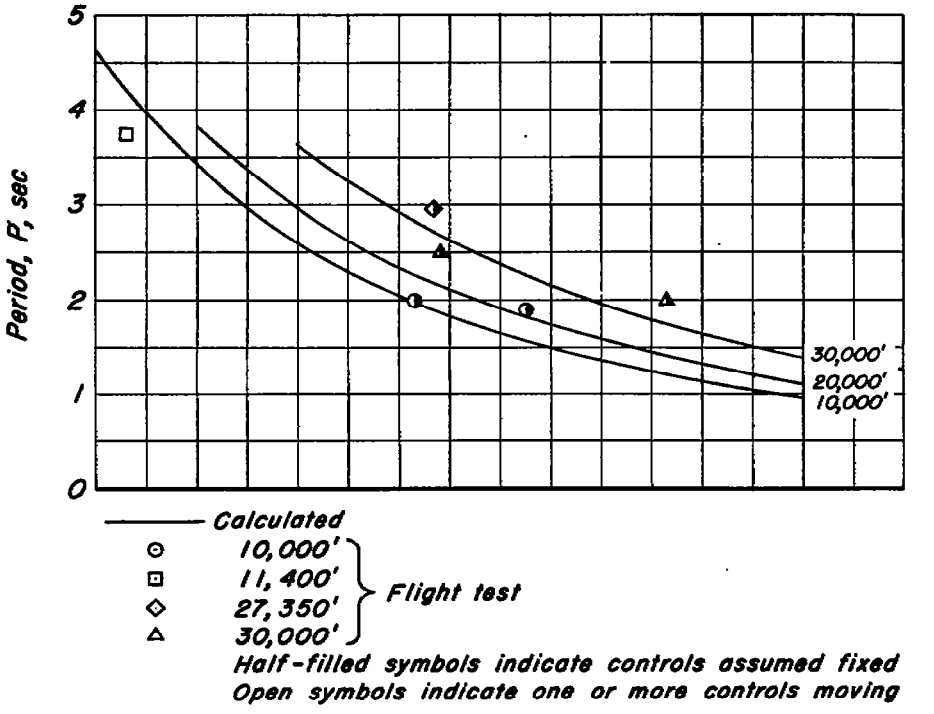

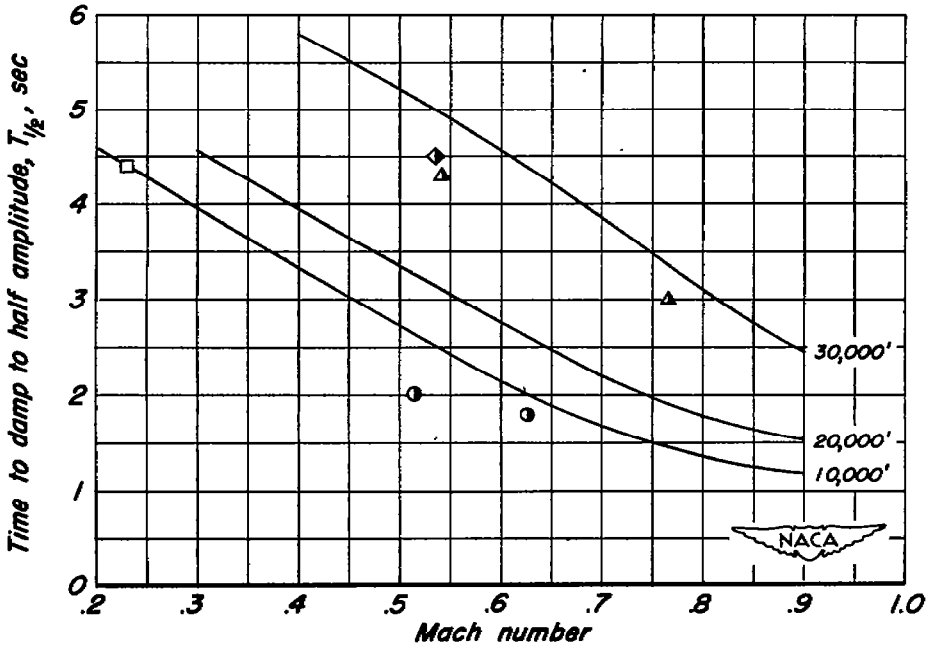

Figure 10.–Variation of period and time to damp to half amplitude with Mach number for airplane H.

[redacted]

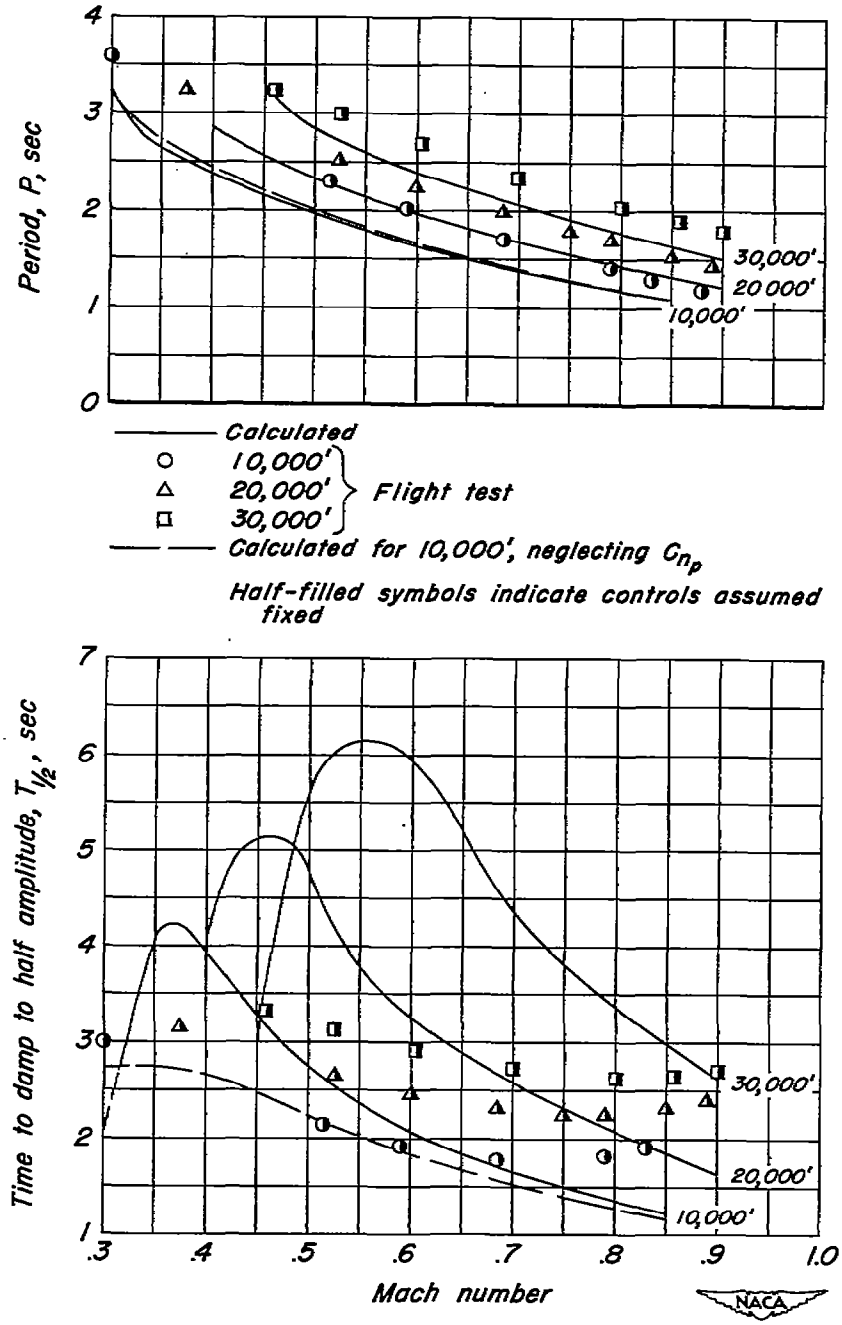

Figure 11.–Variation of period and time to damp to half amplitude with Mach number for airplane I.

[redacted]

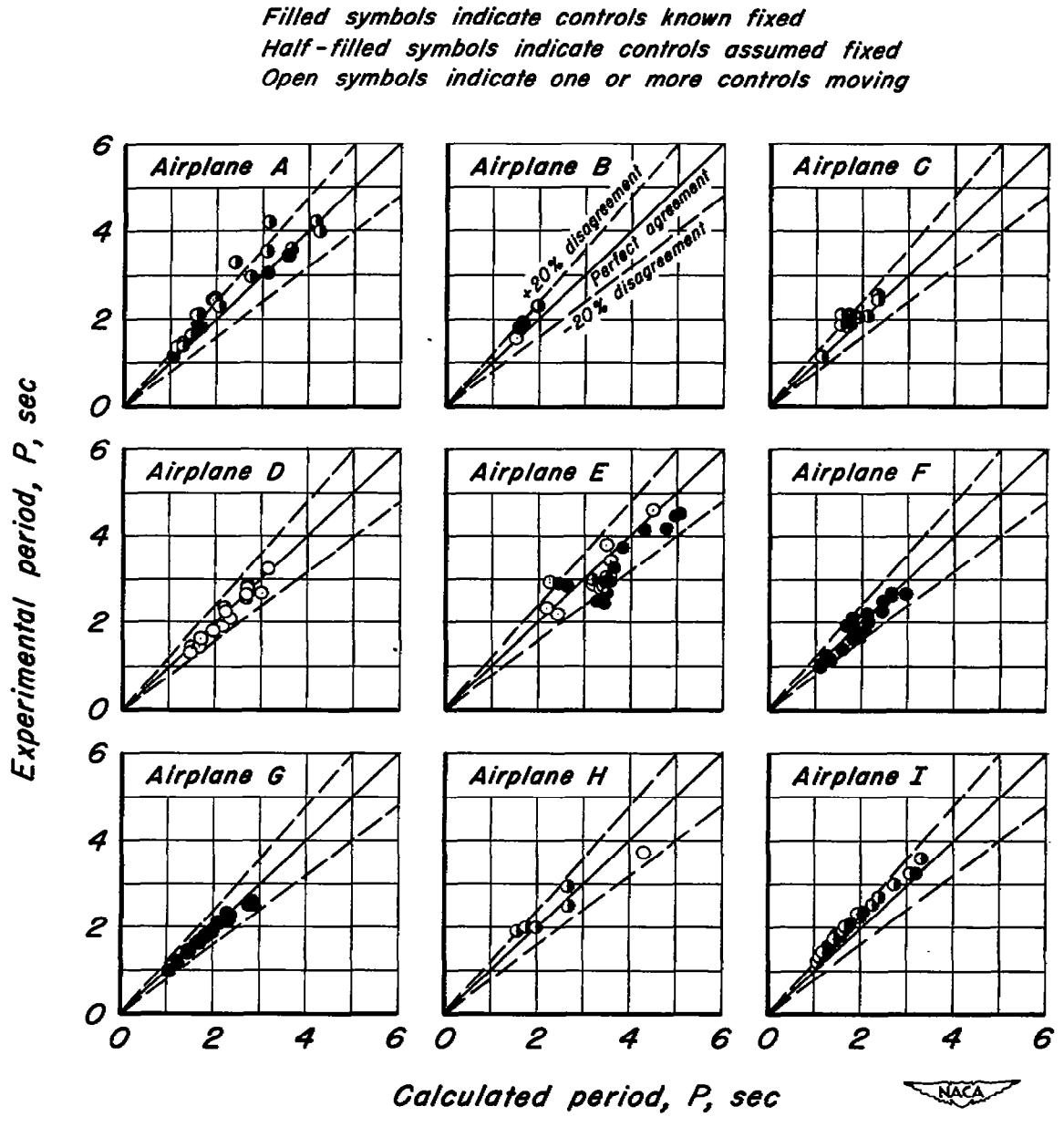

Figure 12.- Comparison between experimental and calculated period for the nine airplanes investigated.

[redacted]

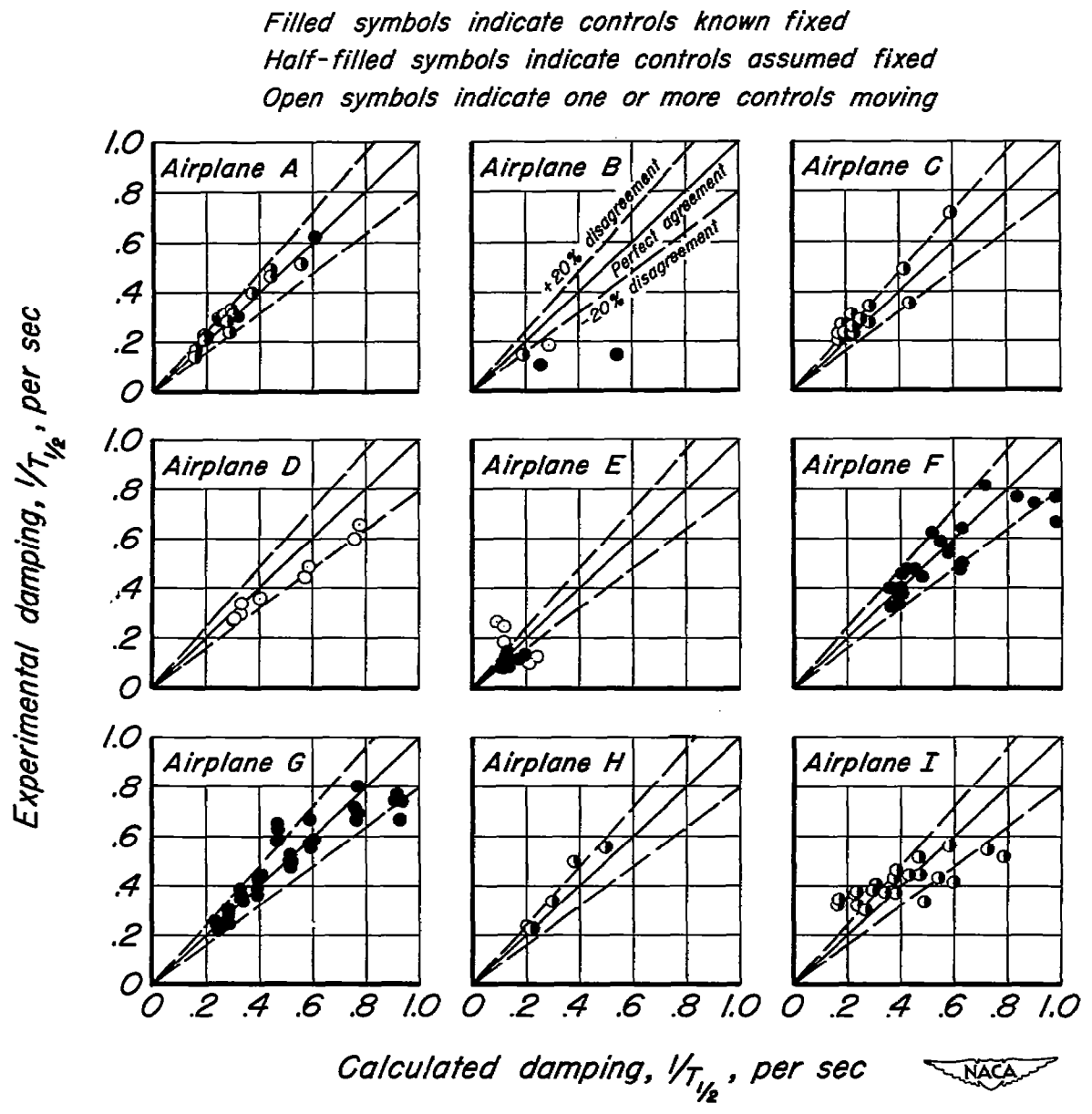

Figure 13.- Comparison between experimental and calculated damping for the nine airplanes investigated.

[redacted]